1538–1553 Nucleic Acids Research, 2011, Vol. 39, No. 4 Published online 5 October 2010
doi:10.1093/nar/gkq854

Structural basis for the dual RNA-recognition modes of human Tra2-β RRM

Kengo Tsuda[1], Tatsuhiko Someya[1], Kanako Kuwasako[1], Mari Takahashi[1], Fahu He[1], Satoru Unzai[2], Makoto Inoue[1], Takushi Harada[1], Satoru Watanabe[1], Takaho Terada[1], Naohiro Kobayashi[1], Mikako Shirouzu[1], Takanori Kigawa[1], Akiko Tanaka[1], Sumio Sugano[3], Peter Güntert[1,4,5], Shigeyuki Yokoyama[1,6,*] and Yutaka Muto[1,*]

[1]RIKEN Systems and Structural Biology Center, [2]Protein Design Laboratory, Yokohama City University, 1-7-29 Suehiro-cho, Tsurumi, Yokohama 230-0045, Japan, [3]Department of Medical Genome Sciences, Graduate School of Frontier Sciences, The University of Tokyo, Tokyo 113-0033, [4]Tatsuo Miyazawa Memorial Program, RIKEN Genomic Sciences Center, Yokohama 230-0045, Japan, [5]Institute of Biophysical Chemistry, Center for Biomolecular Magnetic Resonance, and Frankfurt Institute for Advanced Studies, Goethe-University Frankfurt, Max-von-Laue-Str. 9, 60438 Frankfurt am Main, Germany and [6]Department of Biophysics and Biochemistry, Graduate School of Sciences, The University of Tokyo, Tokyo 113-0033, Japan

Received July 30, 2010; Revised September 8, 2010; Accepted September 11, 2010

ABSTRACT

Human Transformer2-β (hTra2-β) is an important member of the serine/arginine-rich protein family, and contains one RNA recognition motif (RRM). It controls the alternative splicing of several pre-mRNAs, including those of the calcitonin/calcitonin gene-related peptide (CGRP), the survival motor neuron 1 (SMN1) protein and the tau protein. Accordingly, the RRM of hTra2-β specifically binds to two types of RNA sequences [the CAA and $(GAA)_2$ sequences]. We determined the solution structure of the hTra2-β RRM (spanning residues Asn110–Thr201), which not only has a canonical RRM fold, but also an unusual alignment of the aromatic amino acids on the β-sheet surface. We then solved the complex structure of the hTra2-β RRM with the $(GAA)_2$ sequence, and found that the AGAA tetranucleotide was specifically recognized through hydrogen-bond formation with several amino acids on the N- and C-terminal extensions, as well as stacking interactions mediated by the unusually aligned aromatic rings on the β-sheet surface. Further NMR experiments revealed that the hTra2-β RRM recognizes the CAA sequence when it is integrated in the stem-loop structure. This study indicates that the hTra2-β RRM recognizes two types of RNA sequences in different RNA binding modes.

INTRODUCTION

According to various biological circumstances, ~100 regulatory factors control the splicing-site selection on pre-mRNAs, The serine/arginine-rich (SR-rich) proteins are known as splicing regulatory factors. SR-rich proteins have RNA recognition motifs (RRMs) for binding to specific RNA sequences on pre-mRNA, and also contain repeated serine and arginine di-peptides, which are believed to mediate protein–protein interactions for the recruitment of specific initiation factors on the pre-mRNA (1). Consequently, after the SR-rich proteins bind to the specific RNA sequence, they facilitate the binding of initiation factors to the nearby splice sites, and enhance the possible utilization of these sites in the splicing reaction. The specific RNA sequences targeted by the SR-rich proteins are referred to as exonic splicing enhancers (ESEs) (2), because they are located on the exon sequence.

*To whom correspondence should be addressed. Tel: +81 45 503 9165; Fax: +81 45 503 9196; Email: yokoyama@biochem.s.u-tokyo.ac.jp
Correspondence may also be addressed to Yutaka Muto. Tel: +81 45 503 9653; Fax: +81 45 503 9263; Email: ymuto@gsc.riken.jp
Present address:
Tatsuhiko Someya, Graduate School of Life and Environmental Sciences, University of Tsukuba, 1-1-1 Tennodai, Tsukuba-shi, Ibaraki 305-8572, Japan.

The authors wish it to be known that, in their opinion, the first three authors should be regarded as joint First Authors.

© The Author(s) 2010. Published by Oxford University Press.
This is an Open Access article distributed under the terms of the Creative Commons Attribution Non-Commercial License (http://creativecommons.org/licenses/by-nc/2.5), which permits unrestricted non-commercial use, distribution, and reproduction in any medium, provided the original work is properly cited.

Downloaded from nar.oxfordjournals.org at Stadt und Universitatsbibliothek / Section Medizinische Hauptbibliothek on March 1, 2011

The human Transformer2-β (hTra2-β) protein belongs to the SR-rich like (SR-like) protein family (1), and contains one RRM flanked by N- and C-terminal SR-rich regions (Figure 1A). hTra2-β is a homolog of the *Drosophila melanogaster* transformer-2 (Tra2) protein, which plays a significant role in the regulation of male-specific splicing of the doublesex (dsx) pre-mRNA with the transformer (Tra) protein (3). hTra2-β also controls the pre-mRNA splicing of several gene products, such as the calcitonin/calcitonin gene-related peptide (CGRP), the survival motor neuron 1 (SMN1) protein and the tau protein. In many cases, hTra2-β collaborates with other splicing co-regulators (4,5). For instance, the specific binding of hTra2-β to the ESE on exon 7 of the SMN1 pre-mRNA, along with the heterogeneous nuclear ribonucleoprotein-G (hnRNP-G) (6), the splicing factor arginine/serine-rich 9 (SFRS9/Srp30c) (7) and the alternative splicing factor/splicing factor 2 (ASF/SF2) (8,9), is necessary for the inclusion of exon 7 in the mature mRNA. Similarly, the specific binding of hTra2-β to the ESE on exon 10 of the tau pre-mRNA, with ASF/SF2 and SFRS9/Srp30c, is required for the pre-mRNA maturation of the tau protein. The aberrant exclusion of exon 7 from the SMN1 mRNA and that of exon 10 from the tau mRNA produces functionless proteins, resulting in spinal muscular atrophy (SMA) and frontotemporal dementia (FTD), respectively (4,5).

Several RNA sequences have been reported as the targets of the hTra2-β protein. A SELEX experiment revealed that a GAA repeat sequence is a target of the hTra2-β protein (10), and actually this RNA sequence was identified in the ESEs on both exon 7 of the SMN1 pre-mRNA and exon 10 of the tau pre-mRNA. On the other hand, hTra2-β also targets other RNA sequences in addition to the GAA repeat. hTra2-β reportedly interacts with the 13-nt sequence, ACUUCAACAAGUU, on exon 4 of the pre-mRNA of the calcitonin/calcitonin gene-related peptide (CGRP) (11). Accordingly, the *Drosophila* Tra2 protein, a homolog of hTra2-β, binds to the similar 13-nt sequence, UC(U/A)(U/A)C(A/G)AU CAACA, in the female-specific exon 4 of the Drosophila *dsx* gene with the Tra protein (3). As described above, hTra2-β plays significant roles in several alternative-splicing events. However, the binding specificity of the hTra2-β protein still requires clarification. Therefore, the precise RNA recognition mode by the RRM fold of hTra2-β must be elucidated to understand the pathogenic mechanisms of SMA and FTD.

RRMs are widespread in many kinds of eukaryotic RNA binding proteins, and play important roles in sequence-specific RNA binding (12–14). For instance, 901 RRM-containing human proteins are included in the Pfam database release 23.0 (15,16). The canonical RRM consists of a four-stranded anti-parallel β-sheet packed against two α-helices, with a typical βαββαβ topology (14). RRMs contain two well-conserved consensus sequences, termed RNP2 ([I/L/V]-[F/Y]-[I/L/V]-X-N-L) and RNP1 ([K/R]-G-[F/Y]-[G/A]-[F/Y]-[I/L/V]-X-[F/Y]), which correspond to the β1 and β3 strands, respectively

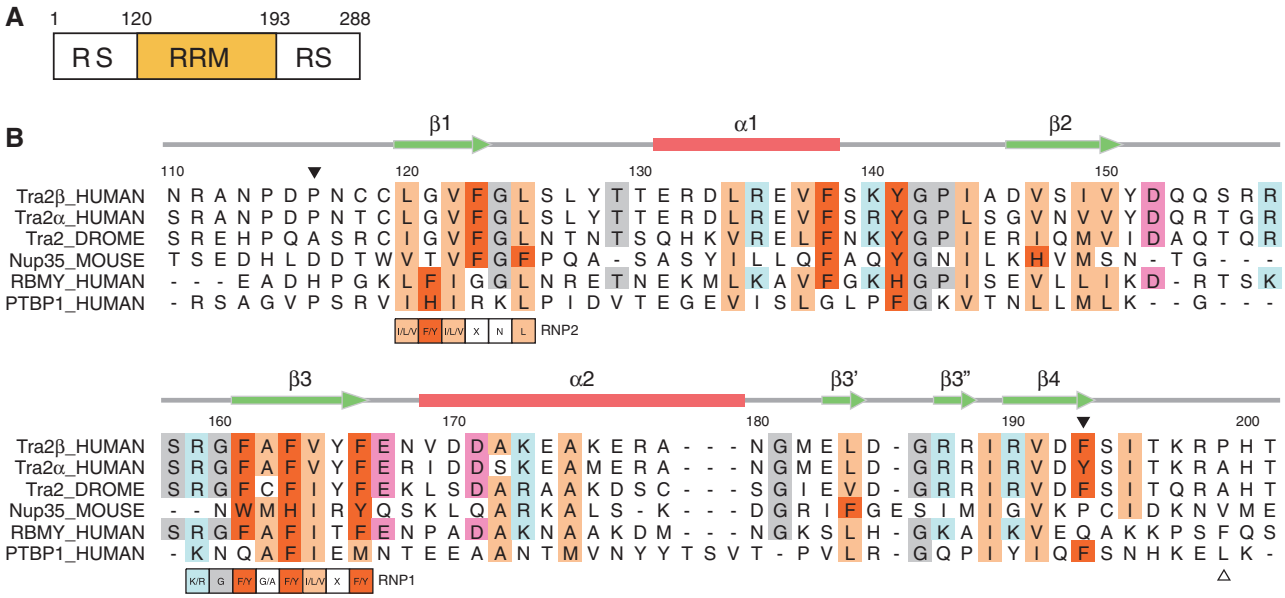

Figure 1. Primary structures of the RRMs of hTra2-β, Nup35, RBMY and PTBP. (**A**) Schematic diagram of the hTra2-β protein. hTra2-β possesses one RRM flanked by the N- and C-terminal SR-rich regions. (**B**) Multiple sequence alignment of the hTra2-β RRM (P62995), the hTra2-α RRM (Q13595), the *Drosophila* Tra2 RRM (P19018), the Nup35 RRM (Q8R4R6), the RBMY RRM (Q15414) and the first RRM domain of PTBP (P26599), based on the 3D structures. Secondary-structure elements are marked by green arrows for β-strands and red bars for α-helices above the sequence alignment. The amino-acid sequences corresponding to RNP1 and RNP2 are indicated by the boxes below the sequences. The amino acids located at the positions of the well-conserved amino acids in the RRM folds are indicated by the colored boxes (aromatic amino acid: red; aliphatic: flesh; positively charged: cyan; negatively charged: pink; G, P and T: gray). The solid black triangles indicate the amino-acid residues interacting with each other for the fixation of the N-terminal extensions, and the open triangle indicates the residue in the C-terminal extension that interacts with the residues located on the β-sheet surface in the hTra2-β RRM.

Downloaded from nar.oxfordjournals.org at Stadt und Universitatsbibliothek / Section Medizinische Hauptbibliothek on March 1, 2011

(17) (Figure 1B). The canonical RRM interacts with the RNA surface through specific hydrogen bonds on its β-sheet surface, and by stacking interactions mediated by the conserved and exposed aromatic rings located on the β1 and β3 strands (14). Interestingly, the putative RRM fold of hTra2-β lacks the typical RNP2 sequence, suggesting a unique RNA recognition mode by hTra2-β (Figure 1B).

In this study, we solved the solution structure of the region spanning residues Asn110–Thr201 of hTra2-β (hereafter, denoted as the hTra2-β RRM), containing the putative RRM fold. Our NMR experiments revealed that the hTra2-β RRM strongly binds to the [5′-(GAAGA A)-3′] sequence, and we subsequently determined the solution structure of the hTra2-β RRM in complex with the [5′-(GAAGAA)-3′] sequence. This defined the specific RNA recognition mechanism of the hTra2-β RRM. Further NMR experiments indicated that a longer RNA segment, containing the CAA sequence, is also recognized by the hTra2-β RRM in a different binding mode. Our study provides significant insight into the dual specificity of RNA sequence recognition by hTra2-β.

MATERIALS AND METHODS

Protein expression and purification

The DNA fragments encoding the RRM fold of hTra2-β (spanning residues Asn110–Thr201 and Arg111–Thr201) (SwissProt accession no. P62995) were subcloned by PCR from the human full-length cDNA clone [hereafter, the regions spanning residues Asn110–Thr201 and Arg111–Thr201 are referred to as the hTra2-β RRM and the hTra2-β RRM-(Arg111–Thr201), respectively]. Each of these amplified DNA fragments was cloned into the expression vector pCR2.1 (Invitrogen), as a fusion with an N-terminal 6-His affinity tag and a TEV protease cleavage site. The $^{13}C/^{15}N$-labeled fusion proteins were synthesized by a cell-free protein expression system (18–20). The reaction mixtures were first adsorbed to a HiTrap chelating column (Amersham Biosciences), which was washed with buffer A (50 mM sodium phosphate buffer, pH 8.0, containing 500 mM sodium chloride and 20 mM imidazole). The proteins were eluted with buffer B (50 mM sodium phosphate buffer, pH 8.0, containing 500 mM sodium chloride and 500 mM imidazole). In order to remove the His-tag, the eluted proteins were incubated at 30°C for 1 h with TEV protease. The tag-free hTra2-β RRMs were further purified by HiTrap Q and HiTrap SP columm chromatography (GE Healthcare).

Nuclear magnetic resonance spectroscopy

For nuclear magnetic resonance (NMR) measurements, the samples were concentrated to 0.8–1.2 mM in 20 mM *d*-Tris–HCl buffer (pH 7.0), containing 100 mM NaCl, 1 mM 1,4-DL-dithiothreitol-d_{10} (*d*-DTT) and 0.02% NaN_3 (in 90% H_2O/10% D_2O), using an Amicon Ultra-15 filter (3000 MWCO, Millipore). NMR experiments were performed at 298 K for the RNA-free form, and at 283 and 298 K for the RNA-bound form on Bruker AV700 and AV800 spectrometers. The ^1H, ^{15}N and ^{13}C chemical shifts were referenced relative to the frequency of the ^2H lock resonance of water. Backbone and side-chain assignments of the hTra2-β RRM were obtained by using a combination of standard triple resonance experiments (21,22). Two-dimensional (2D) [^1H, ^{15}N]-HSQC and three-dimensional (3D) HNCO, HN(CA)CO, HNCACB and CBCA(CO)NH spectra were used to obtain the ^1H, ^{15}N and ^{13}C assignments of the protein backbone. The ^1H and ^{13}C assignments of the non-aromatic side-chains, including all prolines, were obtained using 2D [^1H, ^{13}C]-HSQC, and 3D HBHA(CO)NH, H(CCCO)NH, (H)CC(CO)NH, HCCH-COSY and HCCH-TOCSY spectra. Assignments were checked for consistency with 3D ^{15}N-edited [^1H, ^1H]-NOESY and ^{13}C-edited [^1H, ^1H]-NOESY spectra. The ^1H and ^{13}C spin systems of the aromatic rings of Phe, Tyr and His were identified using 3D HCCH-COSY and HCCH-TOCSY experiments, and 3D ^{13}C-edited [^1H, ^1H]-NOESY was used for the sequence-specific resonance assignment of the aromatic side-chains. A 3D HNHA spectrum was measured to determine the restraints for the ϕ dihedral angle. 3D ^{15}N- and ^{13}C-resolved NOESY spectra were recorded with mixing times of 80 and 150 ms. For the assignments of the RNA molecules, 2D filtered-NOESY spectra with mixing times of 80 and 150 ms and 2D filtered-TOCSY spectra with a mixing time of 43 ms were recorded. The conformation of the sugar rings was identified based on the intensity of the cross peaks between H1′ and H2′ in the 2D filtered-TOCSY spectra. The NMR data were processed using NMRPpipe (23). Analyses of the processed data were performed with the programs NMRView (24) and KUJIRA (25).

For the amide chemical-shift titration experiments, the RNA oligonucleotides {[5′-(GAAGAA)-3′], [5′-(AAAAA A)-3′], [5′-(UCAAU)-3′] and [5′-(GACUUCAACAAGUC)-3′] (Dharmacon)} were dissolved in 20 mM *d*-Tris–HCl buffer (pH 7.0), containing 100 mM NaCl and 1 mM *d*-DTT, to a final RNA concentration of 6 mM. 2D [^1H, ^{15}N]-HSQC spectra were recorded while increasing the concentration of the RNA relative to the hTra2-β RRM solution (200 μM) to a final hTra2-β RRM:RNA ratio of 1:2.

In order to observe the imino proton resonances of the RNA molecules, we performed the 1D NMR measurements and the 2D [^1H, ^1H]-NOESY experiments using the jump-return pulse train (26), at a sample temperature of 283 K.

The measurements of the nitrogen relaxation times, T_1 and T_2, and the ^1H-^{15}N heteronuclear NOE values were performed on a Bruker AV600 spectrometer equipped with a cryo-probe at 298 K, using the ^{15}N, ^{13}C-labeled hTra2-β RRMs in the RNA-free and RNA ([5′-(GAAG AA)-3′])-bound forms at a concentration of 200 μM (27). The eight different values for the relaxation delays were 5, 65, 145, 246, 366, 527, 757 and 1148 ms for measuring ^{15}N T_1 and 32, 48, 64, 80, 96, 112, 128 and 144 ms for ^{15}N T_2. The ^{15}N T_1 and ^{15}N T_2 values were extracted using the curve-fitting subroutine included in the Sparky program (T. D. Goddard and D. G. Kneller, SPARKY 3, University of California, San Francisco, CA, USA). The ^1H-^{15}N heteronuclear NOE values were calculated as the

Downloaded from nar.oxfordjournals.org at Stadt und Universitatsbibiothek / Section Medizinische Hauptbibliothek on March 1, 2011

ratio between the cross-peak intensities with and without ^{1}H saturation. The errors were estimated from the root-mean-square values of the baseline noise in the two spectra (27).

Structure calculations

The 3D structures of the hTra2-β RRM in the RNA-free and RNA-bound forms were determined by combining the automated NOESY cross-peak assignment (28) and the structure calculations with torsion angle dynamics implemented in the program CYANA 2.1 (29,30). Dihedral angle restraints for ϕ were obtained by analyzing the 3D NOESY and 3D HNHA spectra. Restraints for the χ^1 dihedral angles were obtained from the 3D HNHB and HN(CO)HB spectra or by analyzing the pattern of the inter- and intra-NOE intensities (31).

For the determination of the 3D structures of the RNA-bound form, the intermolecular protein-RNA NOEs were manually assigned, using 2D filtered-NOESY spectra. Protein-RNA NOEs from the 2D filtered-NOESY spectrum with a mixing time of 80 ms were divided into two groups with upper distance bounds of 3.5 and 5.0 Å, respectively, according to their intensity. Upper distance bounds of 6.0 Å were applied for the intermolecular NOEs that could only be identified from the 2D filtered-NOESY spectrum with a mixing time of 150 ms (32). In total, 90 intermolecular NOEs between the hTra2-β RRM and RNA were used for the structure calculations.

The structure calculations started from 200 randomized conformers and used the standard CYANA simulated annealing schedule (30), with 40 000 torsion angle dynamics steps per conformer. The 40 conformers with the lowest final CYANA target function values were further refined with the AMBER9 program (33), using an AMBER 2003 force field and a generalized Born solvation model, as described previously (32). The force constants for distance, torsion angle and ω angle restraints were set to 32 kcal mol^{-1} Å^{-2}, 60 kcal mol^{-1} rad^{-1} and 50 kcal mol^{-1} rad^{-2}, respectively. The 20 conformers that were most consistent with the experimental restraints were then used for further analyses. PROCHECK-NMR (34) and MOLMOL (35) were used to validate and to visualize the final structures, respectively.

Estimation of the binding constant by the NMR method

The dissociation constants (K_d) for two RNA fragments, [5′-(AAAAAA)-3′] and [5′-(UCAAU)-3′], were estimated on the basis of the NMR titration experiments. We selected several obvious resonances, with trajectories that could be traced upon the addition of RNA (36). The average amide group chemical shift changes (Δδ) were calculated using Equation (1):

$$\Delta\delta = \sqrt{(\Delta\delta^1\mathrm{H})^2 + \left(\frac{\Delta\delta^{15}\mathrm{N}}{6.5}\right)^2}, \quad (1)$$

where Δ δ^1H and Δ δ^{15}N are the amide proton and amide nitrogen chemical shift differences between the free and RNA-bound states of the protein, respectively. The K_d values were obtained by a nonlinear fit of the NMR chemical shift changes to a simple bimolecular binding model, using Equation (2):

$$\Delta\delta_{obs} = \Delta\delta_{max}\frac{\left\{\left(K_d+(1+r)[P]_0\right) - \sqrt{\left(K_d+(1+r)[P]_0\right)^2 - 4[P]_0^2 r}\right\}}{2[P]_0}, \quad (2)$$

where $\Delta\delta_{obs}$ denotes the observed chemical shift, $\Delta\delta_{max}$ is the maximum chemical shift and $[P]_0$ is the total protein concentration, respectively. In addition, r and K_d denote the hTra2-β RRM/RNA ratio and the dissociation constant of the complex, respectively.

Isothermal titration calorimetry measurements

Isothermal titration calorimetry (ITC) measurements were performed at 25°C by using a Microcal (Amherst, MA) VP-ITC calorimeter. Samples were buffered with 20 mM Tris (pH 7.0), 100 mM NaCl and 1 mM DTT, and were thoroughly degassed before use. At first, a 2.0 ml portion of a 40 μM hTra2-β RRM solution was placed in the cell chamber. Then, a 20-fold higher concentration of four different RNAs, [5′-(GAAGAA)-3′], [5′-(AAAAAA)-3′], [5′-(UCAAC)-3′] and [5′-(GACUUCAACAAGUC)-3′], was injected into the protein solution. The data were analyzed with the Microcal ORIGIN software, assuming a single site binding model. The binding activities of the hTra2-β RRM to the [5′-(AAAAAA)-3′] and [5′-(UCA AC)-3′] sequences were very weak, and the data were not properly fitted when the stoichiometry (n) value was also searched in the fitting analysis. Thus, for the analysis of the K_d values of the [5′-(AAAAAA)-3′] and [5′-(UCA AC)-3′] sequences, we fitted the raw data to a theoretical curve by setting the stoichiometry (n) value to one, and estimated the K_d values.

RESULTS

Solution structure of the hTra2-β RRM

We determined the solution structure of the region spanning Arg111–Thr201 in the hTra2-β protein, which contained the RRM domain [the hTra2-β RRM-(Arg111–Thr201)], by NMR experiments. In total, 1257 NOE distance restraints derived from 3D ^{15}N-edited [^{1}H, ^{1}H]-NOESY and ^{13}C-edited [^{1}H, ^{1}H]-NOESY spectra were assigned and used in the structure calculation, together with 37 dihedral angle restraints (Table 1). The 40 structures obtained from the CYANA calculation were further refined with the AMBER program, resulting in the 20 energy-refined conformers that represent the solution structure of the hTra2-β RRM (Figure 2A). The region spanning Leu120–Phe193 is the core RRM body that adopts the canonical RRM fold, consisting of a four-stranded anti-parallel β-sheet and two α-helices with a βαββαβ topology (β1: Leu120–Phe123, α1: Glu131–Phe138, β2: Asp146–Val150, β3: Phe161–Phe166, α2: Val169–Ala179 and β4: Arg190–Phe193, respectively) (Figures 1B and 2B). In addition, the hTra2-β

Downloaded from nar.oxfordjournals.org at Stadt und Universitatsbibliothek / Section Medizinische Hauptbibliothek on March 1, 2011

Table 1. Structural statistics for the free hTra2-β RRM and its complex with the [5′-(GAAGAA)-3′] RNA

	Free hTra2-β	hTra2-β RRM-$(GAA)_2$ complex	
	RRM	RRM	RNA
NMR restraints			
Distance restraints			
Total NOE	1257	1266	23
Intra-residue	401	386	15
Inter-residue			
Sequential ($\|i–j\| = 1$)	279	287	8
Medium-range ($1 < \|i–j\| < 5$)	181	177	
Long-range ($\|i–j\| \geq 5$)	396	416	
Hydrogen bond restraints[a]	11	11	
Protein–RNA intermolecular		90	
Dihedral angle restraints			
ϕ and ψ	6	15	
χ angle	31	36	
Sugar puckering			2
Structure statistics (40 structures)			
CYANA target function ($Å^2$)	0.02	0.34	
Residual NOE violations			
Number > 0.10 Å	1	4	
Maximum (Å)	0.16	0.34	
Residual dihedral angle violations			
Number > 5.0°	0	0	
Maximum (°)	0.47	2.04	
AMBER energies (kcal/mol)			
Mean AMBER energy	−3752	−5038	
Mean restraints violation energy	2.16	5.56	
Ramachandran plot statistics (%)			
Residues in most favored regions	89.3	91.4	
Residues in additionally allowed regions	10.2	7.8	
Residues in generously allowed regions	0.2	0.8	
Residues in disallowed regions	0.2	0.1	
Average R.M.S.D. to mean structure (Å)			
Protein backbone[b]	0.280	0.242	
Protein heavy atoms[b]	0.947	0.822	
RNA heavy atoms[b]		0.794	
Complex heavy atoms[b]		0.852	

[a]Only used in CYANA calculation.
[b]For residues Leu120–Phe193 of the protein and nucleotides G3–A6 of the RNA.

RRM has an additional β-hairpin, β3′–β3″ (residues: Glu183–Arg188), between helix α2 and strand β4 (Figures 1B and 2B), and a 10-residue loop structure between the β2 and β3 strands (the β2–β3 loop).

As described above, the canonical RRM fold possesses two well-conserved sequences, termed RNP2 and RNP1, which correspond to the β1 and β3 strands, respectively. The consensus RNP2 and RNP1 sequences are defined as [I/L/V]-[F/Y]-[I/L/V]-X-N-L and [K/R]-G-[F/Y]-[G/A]-[F/Y]-[I/L/V]-X-[F/Y]. Based on the present structural information, we found that RNP2 and RNP1 of the hTra2-β RRM have the sequences L-G-V-F-G-L and R-G-F-A-F-V-Y-F, respectively (Figure 1B). The second position of RNP2 is occupied by a Gly residue (Gly121), instead of an aromatic amino acid, while a Phe residue (Phe123) is found at the fourth position of RNP2. Thus, the hTra2-β RRM has an unusual RNP2 sequence (Fig 1B). In RNP1 of the hTra2-β RRM, all of the solvent-exposed amino acids are aromatic amino acids (Figures 1B and 2B).

Consequently, the hydrophobic side-chains of Phe123 (β1), Val150 (β2), Phe161 (β3), Phe163 (β3) and Tyr165 (β3) form a hydrophobic patch on the β-sheet surface of the hTra2-β RRM (Figure 2B). The positively charged amino acids [Arg157 (the β2–β3 loop), Arg159 (the β2–β3 loop), Arg187 (β3″), Arg188 (β3″) and Arg190 (β4)] are gathered at the bottom of the β-sheet surface (Figure 2B and C). This renders the surface of the β-sheet quite suitable for interactions with RNA molecules.

The N- and C-terminal extensions (the regions spanning residues Arg111–Cys119 and Ser194–Thr201, respectively) are unstructured in solution, and the ^1H–^{15}N heteronuclear NOE data indicated that these regions are flexible in the absence of the target RNA molecule, as described below.

Effect of the addition of the [5′-(GAAGAA)-3′] RNA fragment to the hTra2-β RRM

As described above, the SELEX experiment indicated that the $(GAA)_2$ sequence could bind to the hTra2-β RRM-(Arg111–Thr201). Accordingly, upon the addition of [5′-(GAAGAA)-3′] to the hTra2-β RRM-(Arg111–Thr201), some of the main-chain ^1H–^{15}N resonances of the free form gradually disappeared, and correspondingly new resonances of the bound form appeared in the 2D [^1H, ^{15}N]-HSQC spectra (Figure 3A). This indicated that the exchange between the RNA-bound and RNA-free forms is in the intermediate to slow regime on the NMR time scale. A more detailed analysis of the resonances that shifted upon the addition of [5′-(GAAGAA)-3′] revealed that the amino acids on the β-sheet surface of the core RRM body of hTra2-β (especially, Gly124 at the end of the β1 strand and Ile189, Arg190 and Val191 on the β4 strand) were obviously shifted (Figure 4A). Intriguingly, the resonances originating from the N-terminal extension (Ala112, Asn113, Asn117, Cys118 and Cys119) and the C-terminal extension (Ser194, Ile195, Thr196, Lys197 and Arg198) were also strongly affected (Figure 4A), indicating that both the N- and C-terminal extensions contributed to the interaction with [5′-(GAAGAA)-3′]. Based on the ITC experiment, we estimated a K_d value of 1.5 μM for the complex with the [5′-(GAAGAA)-3′] sequence (Supplementary Figure S1A). This clearly indicated that the hTra2-β RRM binds to [5′-(GAAGA A)-3′] tightly enough for the complex structure determination. After considering the possibility that the Arg111 residue in the N-terminal extension may also be involved in the RNA binding, we prepared the protein sample for the region spanning Asn110–Thr201 (the hTra2-β RRM) to analyze the RNA binding activity of hTra2-β.

Solution structure of the hTra2-β RRM in complex with the [5′-(GAAGAA)-3′] RNA fragment

In order to elucidate the RNA recognition mechanism of the RRM fold of hTra2-β, we determined the solution structure of the hTra2-β RRM in complex with the [5′-(GAAGAA)-3′] RNA fragment. Using multidimensional

Downloaded from nar.oxfordjournals.org at Stadt und Universitatsbibliothek / Section Medizinische Hauptbibliothek on March 1, 2011

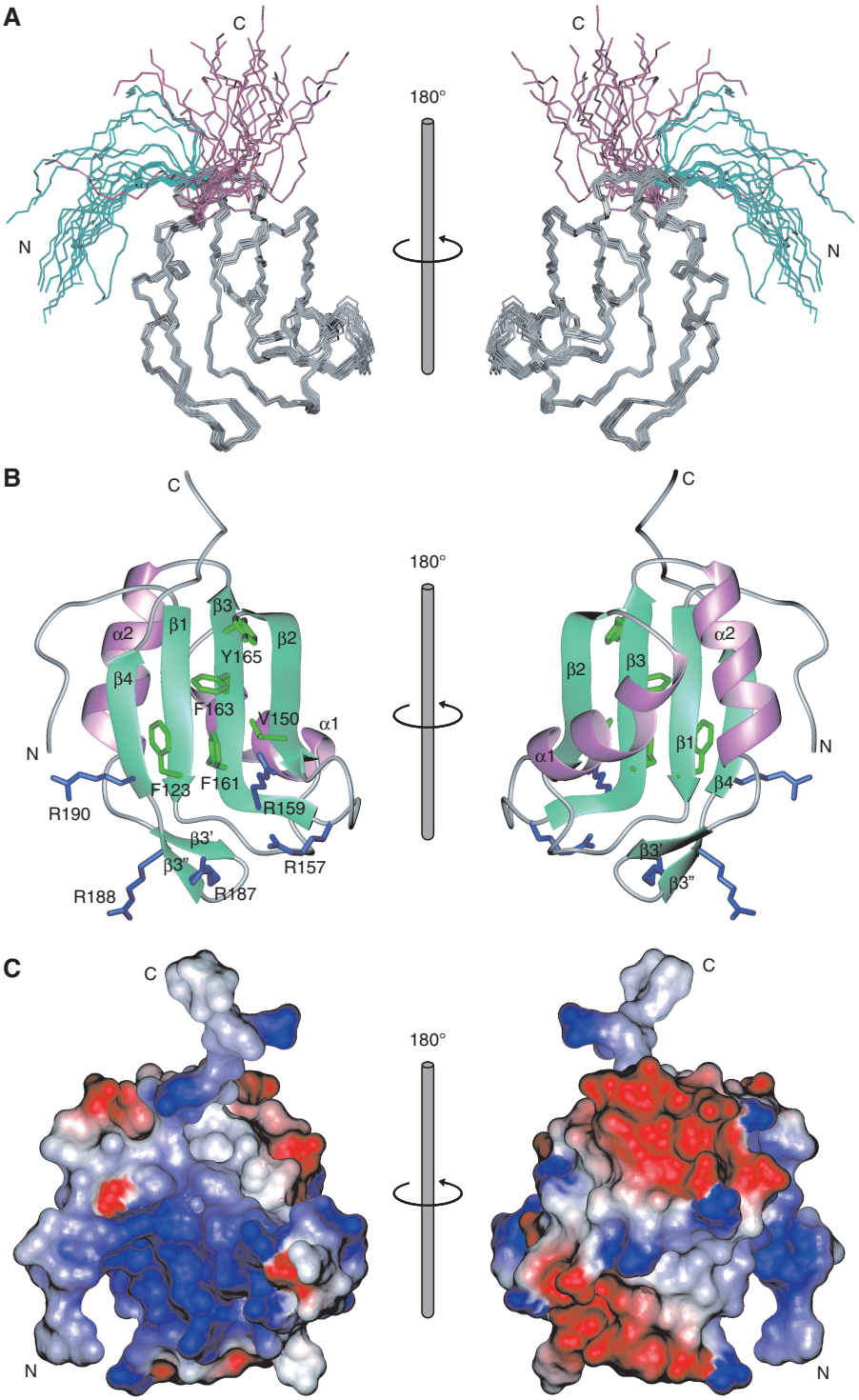

Figure 2. Solution structure of the hTra2-β RRM in the RNA-free form. (**A**) Superposition of the 20 conformers of the hTra2-β RRM (Arg111–Thr201) for the best fit of the backbone atoms of residues Leu120–Phe193. The N-terminal extension (Arg111–Cys119) and the C-terminal extension (Ser194–Thr201) are colored cyan and magenta, respectively. (**B**) Ribbon representation of the hTra2-β RRM. The β-strands and α-helices are colored green and pink, respectively. The side chains of Phe123, Val150, Phe161, Phe163 and Tyr165 are shown in green; and the side chains of Arg157, 159, 187, 188 and 190 are shown in blue. (**C**) Electrostatic potential surface of the hTra2-β RRM. Positively and negatively charged regions are colored blue and red, respectively. All of the structural representations were prepared with the software MOLMOL (35).

heteronuclear NMR spectroscopy, 94.1% of the main-chain resonances and 91.9% of the side-chain resonances of the hTra2-β RRM in the complex were assigned. The solution structure of the complex was determined using 1289 ^{1}H–^{1}H distance restraints from the 2D filtered NOESY, 3D ^{15}N-edited [^{1}H, ^{1}H]-NOESY and ^{13}C-edited [^{1}H, ^{1}H]-NOESY spectra, including 90 inter-molecular and 23 intra-RNA distance restraints (Table 1).

Downloaded from nar.oxfordjournals.org at Stadt und Universitatsbibliothek / Section Medizinische Hauptbibliothek on March 1, 2011

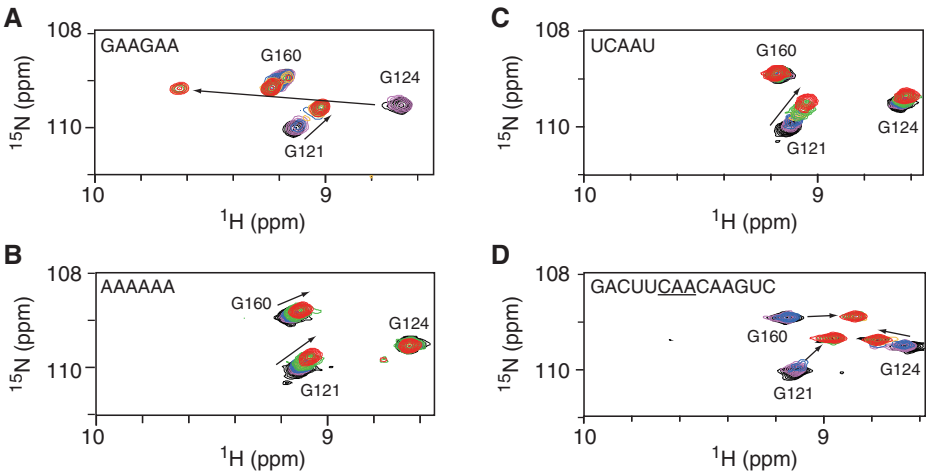

Figure 3. Close-up views of the [^{1}H, ^{15}N]-HSQC spectra of the hTra2-β RRM, showing selected amide shift changes in the absence and presence of the RNAs: (**A**) [5′-(GAAGAA)-3′], (**B**) [5′-(AAAAAA)-3′], (**C**) [5′-(UCAAU)-3′] and (**D**) [5′-(GACUUCAACAAGUC)-3′] [molar ratios of the hTra2-β RRM:RNA were 1:0 (black), 1:0.2 (magenta), 1:0.4 (blue), 1:0.8 (orange), 1:1 (green) and 1:2 (red)].

Among the 200 independently calculated structures, the 40 conformers with the lowest CYANA target function were further refined by restrained energy minimization in the AMBER program (see 'Materials and Methods' section). The 20 conformers that were most consistent with the experimental restraints were used for further analyses.

In the presence of the RNA molecule, the core RRM body (spanning residues Leu120–Phe193) adopts the same structure as in the RNA-free form (Figure 5A). However, the structures of the N- and C-terminal extensions become well-defined in the presence of the RNA molecule, and are involved in the recognition of [5′-(GAAGAA)-3′] (Figure 5A and C). Namely, in the presence of the RNA molecule, the C-terminal extension crosses over the β-sheet surface of the hTra2-β RRM, and a pocket is formed between the C-terminal extension and the β-sheet surface. In addition, the N-terminal extension passes just behind the starting point of the C-terminal extension, and folds back on the β-sheet surface to interact with the RNA molecule (Figure 5A and C). This structural information is consistent with the result of the NMR titration experiment. Thus, we elucidated that the hTra2-β RRM interacts with [5′-(GAAGAA)-3′] on its β-sheet surface, and that both the N- and C-terminal extensions adopt specific structures for the recognition of the RNA molecule.

The NMR relaxation experiments indicated that in the RNA-free form, both the N- and C-terminal extensions of the hTra2-β RRM are flexible, as compared to the core RRM body (without the region corresponding to the β2–β3 loop), because the ^{1}H–^{15}N heteronuclear NOE values for the N- and C-terminal extensions were low (black marks in Supplementary Figure S2). However, in the RNA-bound form, the ^{1}H–^{15}N heteronuclear NOE values for the N- and C-terminal extensions approached those observed for the core RRM body (red marks in Supplementary Figure S2), confirming that the presence of the RNA induced ordered structures in both the N- and C-terminal extensions of the hTra2-β RRM.

Sequence-specific RNA recognition mechanism of the AGAA sequence by the hTra2-β RRM

In the structure of the complex between the hTra2-β RRM and the [5′-(GAAGAA)-3′] RNA, the four base moieties (A3, G4, A5 and A6) contact the β-sheet surface (Figure 5). In contrast, the positions of G1 and A2 are undefined, and thus these two nucleotides were not recognized by the hTra2-β RRM. These structural features are supported by the NOE information (Table 1).

The A3 base moiety is located in the space between the side chains of Arg187 and Arg190 (the β3″ strand), and is stacked with the guanidyl group of Arg190 (Figure 5D, left). In addition, the A3 base moiety contacts the main chain of Gly124 by van der Waals interactions (Figure 5D, left). Furthermore, an intermolecular hydrogen bond may exist between the side chain of Arg190 and the O2′ of the sugar moiety of A3 (Figure 5D, left). The guanidyl group of Arg187 probably forms hydrogen bonds with the backbone phosphate between A2 and A3 (Figure 5D, left). The A3-binding site probably has the plasticity needed for the base recognition, since it was difficult to confirm the presence of direct hydrogen bonds between the A3 base moiety and the hTra2-β RRM. However, the replacement of the adenine base with a guanine base would cause steric hindrance between the 2-amino group of the guanine base and the backbone atoms of the β4 strand [such steric hindrance around the 2-amino group of a guanine base was frequently observed in the discrimination between adenine and guanine bases (37)]. Moreover, an informatics analysis supports the preference of an adenine base over a guanine base by an Arg residue as a stacking partner (37). Thus, the adenosine base seems to fit well into the space between Arg188 and Arg190.

The G4 base moiety is stacked with the aromatic ring of Phe123 as well as the side chain of Arg111 on the N-terminal extension, and is recognized by base-specific hydrogen bonds with the side chains of Arg190 and Asp192 (Figure 5D, middle). The A5 base moiety makes

Downloaded from nar.oxfordjournals.org at Stadt und Universitatsbibliothek / Section Medizinische Hauptbibliothek on March 1, 2011

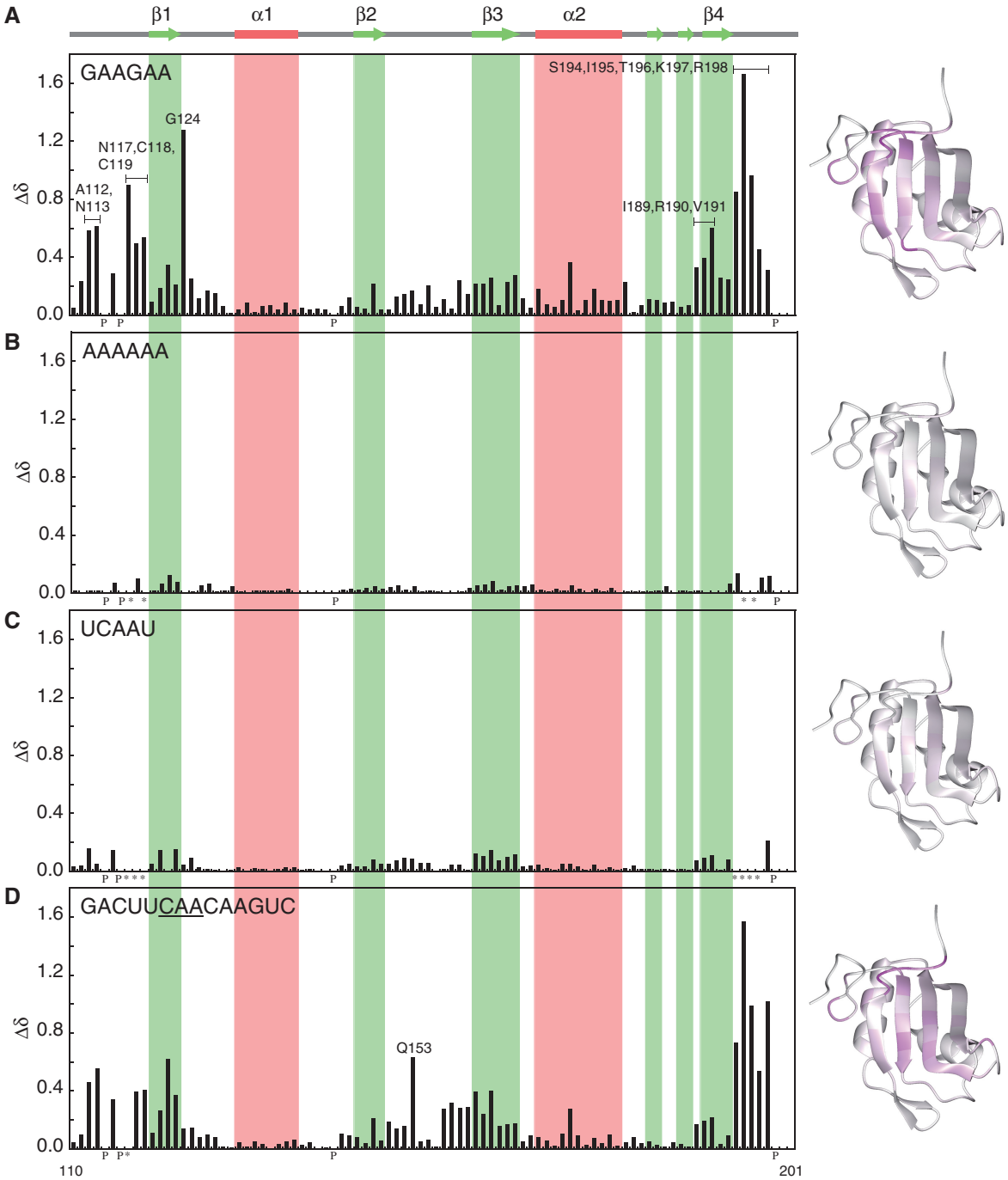

Figure 4. NMR chemical shift perturbations of the hTra2-β RRM upon RNA binding (protein:RNA ratio = 1:1). (**A**) [5′-(GAAGAA)-3′], (**B**) [5′-(AAAAAA)-3′], (**C**) [5′-(UCAAU)-3′] and (**D**) [5′-(GACUUCAACAAGUC)-3′]. Left panels: Plot of the magnitudes of the chemical shift change on the vertical axis, and the amino acid residue numbers on the horizontal axis. Right panels: Chemical shift perturbations mapped on the tertiary structure of the hTra2-β RRM. The chemical shift perturbation values were obtained from the [^{1}H, ^{15}N]-HSQC spectrum. The absolute values of the chemical shift change Δδ were calculated as follows: $\Delta\delta = [(\Delta\delta_{15N}/6.5)^2+\Delta\delta_{1H}^2]^{1/2}$. Amino acid residues with significant chemical shift changes are labeled. Residues with resonances that could not be assigned after the addition of the RNA are indicated by asterisks.

van der Waals interactions with the side chains of Arg111 in the N-terminal extension, Phe123 and Phe163 on the β-sheet surface, and Ile195 in the C-terminal extension. Base-specific hydrogen bonds with the Hoogsteen edge of the A5 base moiety were found between the amino group of the A5 base moiety and the carbonyl oxygen of Phe193, as well as between the N7 atom of the A5 base and the amide proton of Ile195. An adenine base at the A5 position seems more suitable than a guanine base, because a guanine base could not form the hydrogen bond with the carbonyl oxygen of Phe193. In addition, an intramolecular hydrogen bond is formed between the amino group of the G4 base moiety and the N1 atom of the A5 base moiety (Figure 5D, middle). This base-specific hydrogen-bond

Downloaded from nar.oxfordjournals.org at Stadt und Universitätsbibliothek / Section Medizinische Hauptbibliothek on March 1, 2011

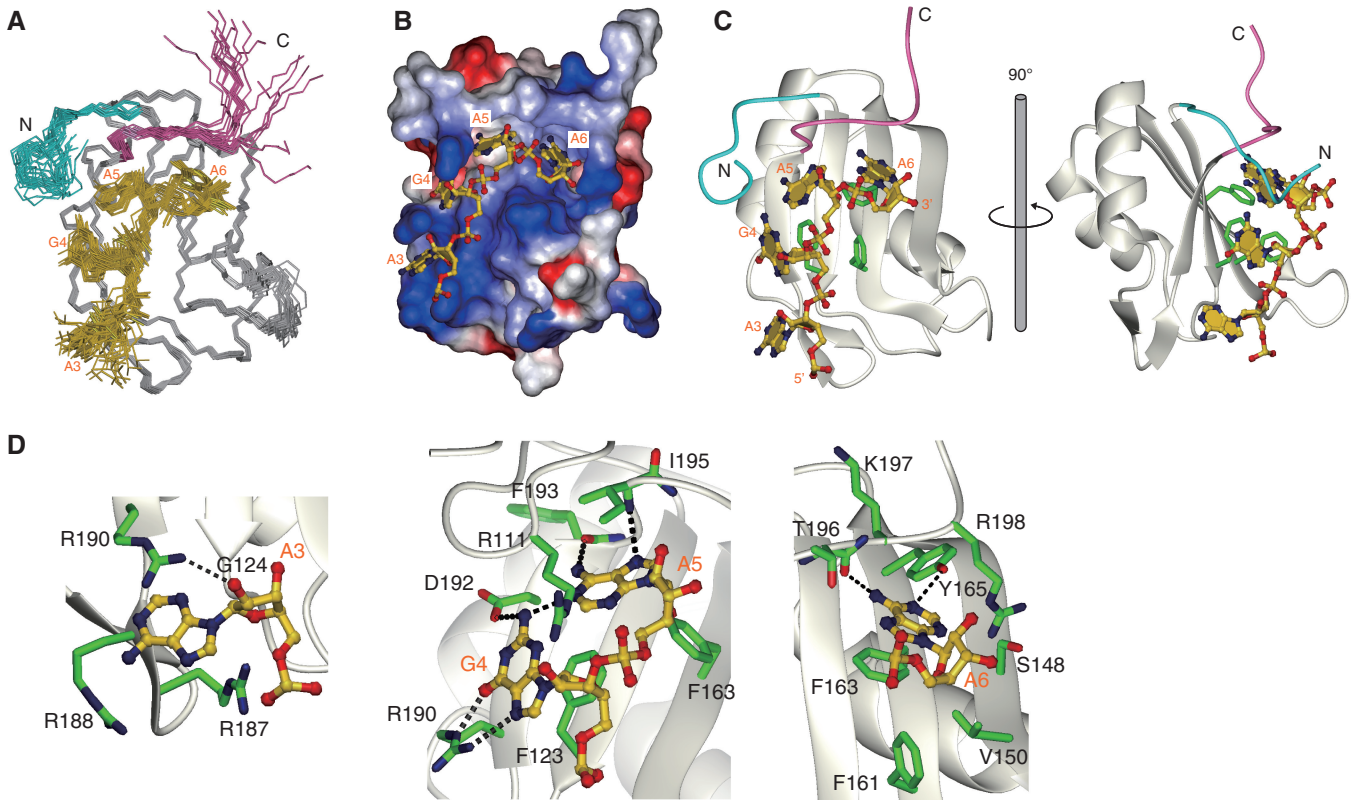

Figure 5. Solution structure of the hTra2-β RRM-[5′-(GAAGAA)-3′] complex. (**A**) Backbone traces of the 20 conformers of the hTra2-β RRM complex. The protein structures are shown in the same orientation as that of the free form of the hTra2-β RRM in Figure 2. Within the RNA molecules, the well-structured AGAA sequence (corresponding to A3–A6) is shown in gold. (**B**) Electrostatic potential surface of the hTra2-β RRM-[5′-(GAAGAA)-3′] complex. The atoms of the RNA molecule are shown in red (oxygen), blue (nitrogen) and gold (other heavy atoms). (**C**) Ribbon representation of the hTra2-β RRM-[5′-(GAAGAA)-3′] complex. The atoms of the RNA molecule are shown as in (B). (**D**) Close-up views of the RNA recognition by the hTra2-β RRM. On the ribbon representation of the backbone of protein, the side chains for the RNA recognition in the hTra2-β RRM and the RNA molecule are colored green for carbons in the protein, red for oxygens, and blue for nitrogens. The RNA molecule is shown as in (B). The hydrogen bonds were calculated by MOLMOL, and are represented by black dashed lines.

network clarifies the preference for the G–A sequence by the hTra2-β RRM.

Finally, the A6 base moiety protrudes into the pocket formed by the side chains of Ser 148, Val150, Phe163 and Tyr165 on the β-sheet surface and those of Lys197 and Arg198 in the C-terminal extension (Figure 5D, right). The A6 base moiety is stacked with the aromatic side chain of Phe163 on RNP1 (corresponding to the β3 strand) and can form hydrogen bonds between the carbonyl oxygen of Thr196 and the amino group of the A6 base moiety, and between the N1 of the A6 base moiety and the Hη of Tyr165 (Figure 5D, right). Collectively, these findings indicated that mainly the AGAA nucleotide sequence is specifically recognized by the hTra2-β RRM (see also 'Discussion' section and Figure 5D for details).

Importance of the guanine base in the target RNA sequence

The present structural study indicated the importance of the guanine base moiety for the specific recognition mediated by the hTra2-β RRM. In order to investigate the discrimination between the two purine nucleotides, adenosine and guanosine, by the hTra2-β RRM, we performed the ITC and NMR titration experiments with [5′-(AAAAAA)-3′]. The binding of the hTra2-β RRM to [5′-(AAAAAA)-3′] was very weak, and we could not obtain reliable data for the estimation of the K_d value at the protein and RNA concentrations employed in the ITC experiment (Supplementary Figure S1B). Thus, based on the NMR titration experiment, we found that the exchange between the RNA-bound and RNA-free forms is fast on the NMR time scale (Figure 3B). We selected three residues, Gly121, Phe123 and Tyr151, and based on the NMR titration experiment, estimated a K_d value for [5′-(AAAAAA)-3′] of over 100 μM (Gly121: 170.1 μM, Phe123: 126.1 μM and Tyr151: 173.2 μM). A comparison of the magnitudes of the chemical shift changes between [5′-(GAAGAA)-3′] and [5′-(AAAAAA)-3′] at a protein:RNA molar ratio of 1:1 revealed that the chemical shift changes for [5′-(AAAAAA)-3′] are much smaller than those for [5′-(GAAGAA)-3′] (Figure 4A and B). Thus, the binding activity of the hTra2-β RRM for [5′-(AAAAAA)-3′] is much weaker than that for [5′-(GAAGAA)-3′]. On the basis of the complex structure, we pointed out that the G4 base moiety in the [5′-(GAAGAA)-3′] sequence plays a crucial role in fixing the A5 base moiety on the

Downloaded from nar.oxfordjournals.org at Stadt und Universitatsbibliothek / Section Medizinische Hauptbibliothek on March 1, 2011

hTra2-β RRM. The titration experiments confirmed that the GA di-nucleotide is the key sequence element for tight binding.

Recognition of the [5′-(UCAAU)-3′] sequence by the hTra2-β RRM

As described above, besides the $(GAA)_2$ sequence, hTra2-β also interacts with the 13-nt sequence, ACUUC AACAAGUU, on exon 4 in the pre-mRNA of CGRP (11), and the *Drosophila* Tra2 protein binds to a similar 13-nt sequence, UC(U/A)(U/A)C(A/G)AUCAACA, in the female-specific exon 4 of the Drosophila *dsx* gene (3). Considering the common features of these two 13-nt sequences and the similarity to the GAA sequence, the CAA sequence could be another candidate target sequence of hTra2-β. Therefore, we performed the NMR titration experiment for [5′-(UCAAU)-3′]. Upon an increase of the protein:RNA molar ratio from 1:0 to 1:2, some resonances shifted in a continuous manner (Figure 3C). The exchange between the [5′-(UCAAU)-3′] RNA-bound and RNA-free forms was fast on the NMR time scale, similar to the case of [5′-(AAAAAA)-3′] (Figures 3B, C, and 4B and C). The NMR titration experiment yielded a K_d value for the hTra2-β RRM: [5′-(U CAAU)-3′] RNA complex of ~40 μM (Gly121: 34.6 μM, Phe123: 44.5 μM and Tyr151: 42.9 μM). We obtained almost the same K_d value (47.8 μM) from the ITC experiment (Supplementary Figure S1C). The magnitude of the chemical shift changes for [5′-(UCAAU)-3′] at a protein:RNA molar ratio of 1:1 are small as compared to those for [5′-(GAAGAA)-3′], and are comparable to those for [5′-(AAAAAA)-3′] (Figure 4A–C). Thus, the binding of the short [5′-(UCAAU)-3′] sequence to the hTra2-β RRM was weaker, as compared to that of the [5′-(GAAGAA)-3′] sequence. The [5′-(UCAAU)-3′] sequence contains the AA dinucleotides, which could fit well in the AA recognition site on the β-sheet surface of the hTra2-β RRM. However, the cytidine nucleotide preceding the AA dinucleotides appears to be insufficient to fix the A3 nucleotide of [5′-(UCAAU)-3′] on the β-sheet surface, as in the [5′-(AAAAAA)-3′] sequence.

Different RNA-binding mode for the CAA sequence by the hTra2-β RRM

In order to find additional factors facilitating the interaction between the hTra2-β RRM and the CAA sequence, we analyzed the 13-mer RNA sequence on exon 4 in the pre-mRNA of CGRP, ACUUCAACA AGUU, with the Mfold program (38,39), which suggested that this 13-mer sequence potentially adopts a stem-loop structure. Expecting a more stable stem structure, we performed several NMR experiments with the similar 14-mer RNA sequence, GACUUCAACAAGUC. In the 1D jump-and-return spectra for the 14-mer RNA molecule, we observed five imino proton resonances, two sharp ones and three broad and ambiguous ones (Supplementary Figure S3A, top). NOEs between these imino protons were observed in 1D-NOE and 2D [^{1}H, ^{1}H]-NOESY experiments with the jump-and-return pulse train, which revealed that A2–U13 and C3–G12 formed stable core base pairs. In addition, other weak base pairs are formed around the core base pairs (Supplementary Figure S3C). As deduced from the Mfold program, the 14-mer RNA fragment could adopt the stem-loop structure, and the CAAC sequence in the 14-mer RNA fragment might be located within the loop region (Supplementary Figure S3C), although the base pairs in the stem structure seem to be weak.

After the addition of the hTra2-β RRM to the 14-mer RNA molecule, at a molar ratio of 1:1, we also observed five imino proton resonances (Supplementary Figure S3A, bottom). The assignments of these resonances were confirmed by the 1D NOESY and the 2D [^{1}H, ^{1}H]-NOESY experiments. The four imino proton resonances of U4, U5, G12 and G13 were clear, while that of G1 was broad (Supplementary Figure S3A, bottom; and Figure 3B, right). The chemical shift values for the imino protons of G1, G12 and U13 did not change between the protein-free and protein-bound forms. This indicated that the stem-loop structure of the 14-mer RNA is stabilized upon binding to the hTra2-β RRM.

We performed the NMR titration experiment for the 14-mer RNA molecule. Interestingly, although the 14-mer RNA lacked GAA tri-nucleotides in the loop region, the [5′-(GACUUCAACAAGUC)-3′] sequence strongly affected the protein resonances in the 2D [^{1}H, ^{15}N]-HSQC spectra (Figure 3D). The chemical shift changes were similar to those for the [5′-(GAAGAA)-3′] sequence, and the amino acids on the N- and C-terminal extensions were also significantly affected (Figures 3A and 4A; 3D and 4D). On the other hand, a detailed analysis of the chemical shift changes revealed that the effects on Gly124 and the amino acid residues on the β4 strand (Ile189–Val191) were significantly smaller than for the [5′-(GAAGAA)-3′] sequence (Figure 4A and D). Instead, the amino acid residues on the β2–β3 loop region, especially Gln153, were strongly affected by the addition of the [5′-(GACUUCAACAAGUC)-3′] RNA (Figure 4D). ITC experiments yielded a K_d value of 3.48 μM for [5′-(GACU UCAACAAGUC)-3′] (Supplementary Figure S1D), in good agreement with the NMR titration experiments. Therefore, we conclude that the hTra2-β RRM can efficiently recognize the CAA sequence when it is integrated in the stem-loop structure.

DISCUSSION

Role of the N- and C-terminal extensions in RNA binding by the hTra2-β RRM

When an RRM binds to the target RNA molecule, other regions besides the core RRM body are involved in the RNA recognition in several cases, such as the C-terminal extension for Fox-1 (40) and U1A (41), the N-terminal extension for the CUG-BP1 RRM3 (32), and both the N- and C-terminal extensions for the hnRNP A1 RRM1 (42) and the RRM1 of poly pyrimidine-tract binding protein (the PTBP RRM1) (43). Structural similarity was especially observed in both the N- and C-terminal extensions between the PTBP RRM1 and the hTra2-β RRM, when they were bound to their target RNAs

Downloaded from nar.oxfordjournals.org at Stadt und Universitatsbibliothek / Section Medizinische Hauptbibliothek on March 1, 2011

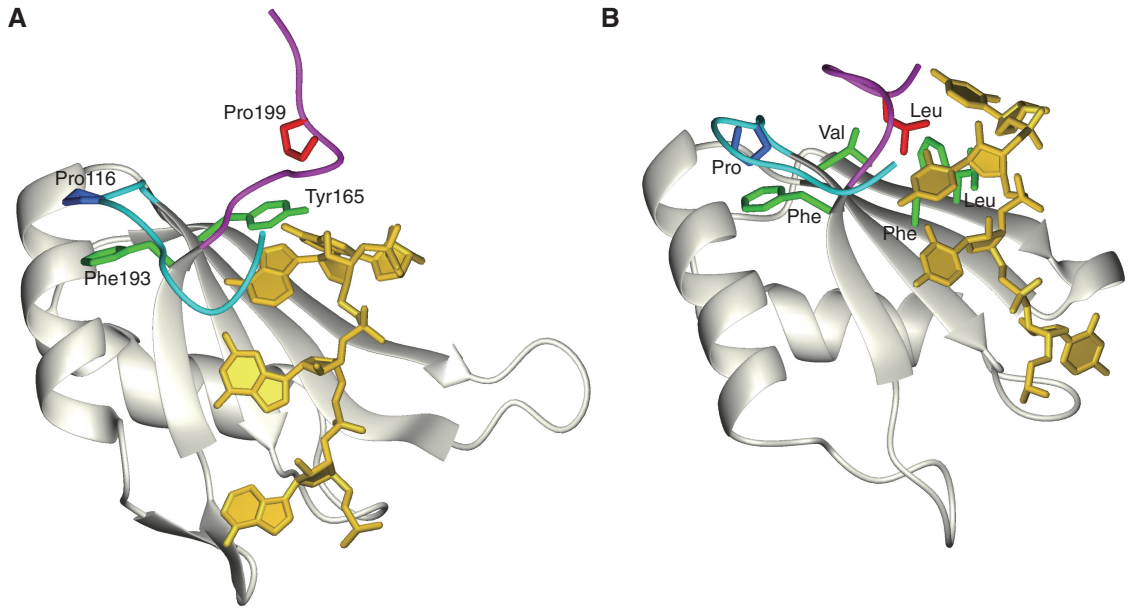

Figure 6. Comparison of ribbon representations of the hTra2-β RRM in complex with [5′-(GAAGAA)-3′] RNA (**A**); and the first RRM domain of poly pyrimidine-tract binding protein (PTBP RRM1) (PDBID: 2AD9) (**B**). In both structures, the N-terminal extension is colored cyan (the side-chain of the Pro residue in the N-terminal extension is depicted in blue), and the C-terminal extension is colored magenta (the side chain of Pro199 of the hTra2-β RRM, and the Leu residue of the PTBP RRM1 in the C-terminal extension are depicted in red). The side chain of the aromatic ring residue located at the end of the β4 strand and the side chains interacting with the residue in the C-terminal extension on the β-sheet surface are depicted in green. The RNA molecule is shown in gold.

(Figure 6B). In the PTBP RRM1, even without an RNA molecule, the C-terminal extension is fixed on and traverses the β-sheet surface of the core RRM body, because the hydrophobic aliphatic amino acid residue (Leu) in the C-terminal extension interacts with the hydrophobic residues on the β-sheet surface (Figures 1B and 8B). When the target RNA molecule is located on the β-sheet surface, several carboxyl oxygens and/or amide protons of the C-terminal extension are involved in the recognition of the poly-pyrimidine tracts. On the other hand, in the case of the hTra2-β RRM, there are no hydrophobic aliphatic amino acid residues on the C-terminal extension, corresponding to the above-mentioned Leu residue of the PTBP RRM1, for the interaction with the amino acid residues on the β-sheet surface. Therefore, without the RNA molecules, the C-terminal extension is rather flexible and does not closely contact the β-sheet surface. However, in the presence of the RNA molecule, Pro199 in the C-terminal extension forms a van der Waals contact with the aromatic ring of Tyr165 on the β-sheet surface (Figure 6A), and the C-terminal extension adopts a similar conformation as seen in the PTBP RRM1 for the recognition of the base moieties of the RNA molecule (Figure 6A and B).

Simultaneously, in the cases of both the hTra2-β RRM and the PTBP RRM1, several amino acid residues on the N-terminal extension cover the nucleotides. Interestingly, the hTra2-β RRM and the PTBP RRM1 share common structural features around the root of the N-terminal extensions: the presence of the Pro residue in the N-terminal extension [corresponding to Pro116 in the hTra2-β RRM (Figure 1B)], and that of the Phe residue at the end of the β4 strand (corresponding to Phe193 in the hTra2-β RRM) (Figure 8A and B). The hydrophobic interactions between these residues facilitate the folding of the N-terminal extension back onto the β-sheet surface, which mediates the RNA recognition (Figure 8A and B).

Role of the aromatic amino acid residue with the unusual alignment on the β-sheet surface

In the case of the hTra2-β RRM, the alignment of the aromatic amino acid residues (Phe123, Phe161, Phe163 and Tyr165) on the β-sheet surface is unusual, as compared to that in the canonical RRMs, and the amino-acid sequence of the β1 strand (RNP2) is distinct from the consensus RNP2 sequence (Figure 7B, top). In the canonical RRM, the second position of the β1 strand is occupied by an aromatic amino acid residue, and the fourth position contains a small amino acid residue, such as Gly (as a representative canonical RRM, the RRM of the RNA binding motif Y (RBMY) protein is shown in Figure 7C, top). In contrast, in the hTra2-β RRM, the second and fourth positions are occupied by Gly121 and Phe123, respectively (Figure 7B, top).

A search of the structural database revealed that the atypical RRM domain of the mouse Nup35 protein also has the same aromatic alignment on its β-sheet surface (Figure 7A, top) (44). However, the Nup35 RRM reportedly lacks RNA binding activity. Instead, it mediates protein-protein interactions and acts as a homodimerization domain (Figure 7A, middle and bottom). For the homodimerization, the aromatic rings of the Phe residue at the fourth position of the β1 strand and the Trp

Downloaded from nar.oxfordjournals.org at Stadt und Universitatsbibliothek / Section Medizinische Hauptbibliothek on March 1, 2011

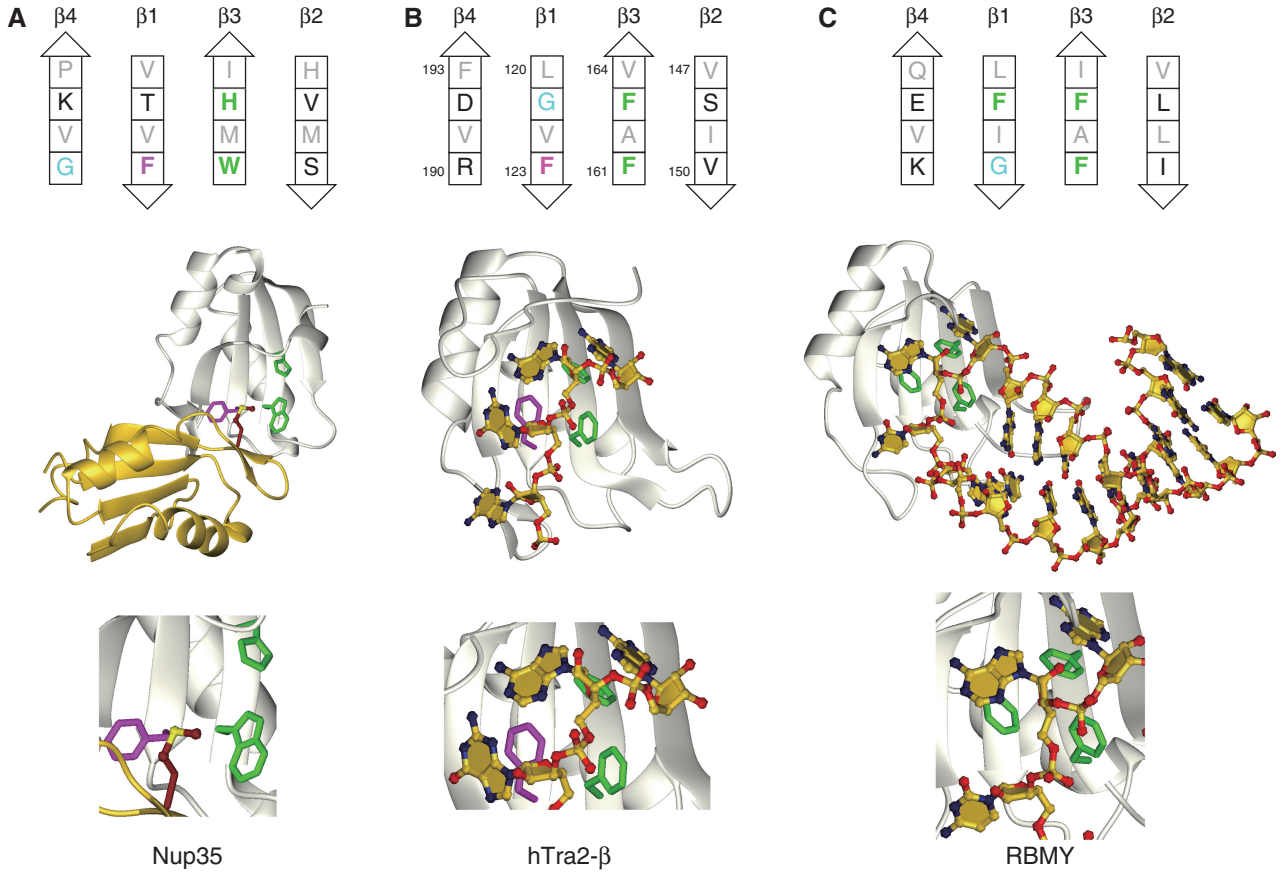

Figure 7. Comparison between the Nup35 RRM (PDBID: 1WWH) (**A**), the hTra2-β RRM (**B**) and the RBMY RRM (PDBID: 2FY1) (**C**). Top panel: Schematic representation of the amino acids on the β-sheet surface for the Nup35 RRM, the hTra2-β RRM and the RBMY RRM. Solvent-exposed amino acids are colored black, glycine residues are cyan, and aromatic amino acids are green or magenta. Amino acids involved in the core formation are indicated by faint colors. Middle panel: Ribbon representations of the tertiary structures of the homodimerized Nup35 RRM, the hTra2-β RRM in complex with [5′-(GAAGAA)-3′], and the RBMY RRM in complex with the target RNA molecule. Bottom panel: Close-up view of the interaction site on the β-sheet surface with the target molecules for the Nup35 RRM, the hTra2-β RRM and the RBMY RRM. The aromatic side chains, colored green or magenta in the top panel, are shown on the tertiary structures in the middle and bottom panels.

residue at the first position of the β3 strand face each other to form a concave surface, for the accommodation of the side chain of the Met residue on the other Np35 molecule (Figure 7A, middle and bottom). Thus, the aromatic concave surface mediates the protein-protein interactions (Figure 7A, middle and bottom). On the other hand, in the complex structure between the hTra2-β RRM and the [5′-(GAAGAA)-3′] RNA sequence, the χ^1 angle of Phe123 in the hTra2-β RRM (−60°) is different from that of the corresponding Phe residue in the Nup35 RRM (+60°) (Figure 7A and B, bottom). Therefore, Phe123 of the hTra2-β RRM cannot form a concave surface with the Phe residue at the first position of the β3 strand. Accordingly, in the hTra2-β RRM, the aromatic ring of Phe123 interacts with that of Phe163, located at the third position of the β3 strand, to form a convex surface that stacks with the base moieties of the GAA tri-nucleotides (Figure 7B, middle and bottom).

The position of the Gly residue on the β-sheet surface might play a significant role in the control of the χ^1 angle of the Phe residues at the fourth position of the β1 strand, for both the Nup35 RRM and the hTra2-β RRM. In the Nup35 RRM, the Gly residue is located at the first position of the β4 strand (on the left side of the discussed Phe residue) (Figure 7A, top). On the other hand, in the hTra2-β RRM, the Gly residue is located at the second position of the β1 strand, two residues apart from Phe123 in the same strand (Figure 7B, top). Consequently, the aromatic ring of this Phe residue occupies the space just above the Gly residue. In order to avoid steric hindrance on the β-sheet surface, the χ^1 angle of Phe123 in the hTra2-β RRM and that of the corresponding Phe residue in the Nup35 RRM are −60° and +60°, respectively (Figure 7A and B).

Recognition of the consecutive purine bases by the hTra2-β RRM

As described above, two well-conserved aromatic amino-acid residues are present in the centers of both RNP2 and RNP1 in the canonical RRM, respectively. A survey of the RNA recognition mode by RRM (45) revealed that consecutive nucleotides (5′-[N1–N2]-3′) are normally stacked with these aromatic side-chains; for instance, N1 was stacked with the aromatic amino-acid

Downloaded from nar.oxfordjournals.org at Stadt und Universitatsbibliothek / Section Medizinische Hauptbibliothek on March 1, 2011

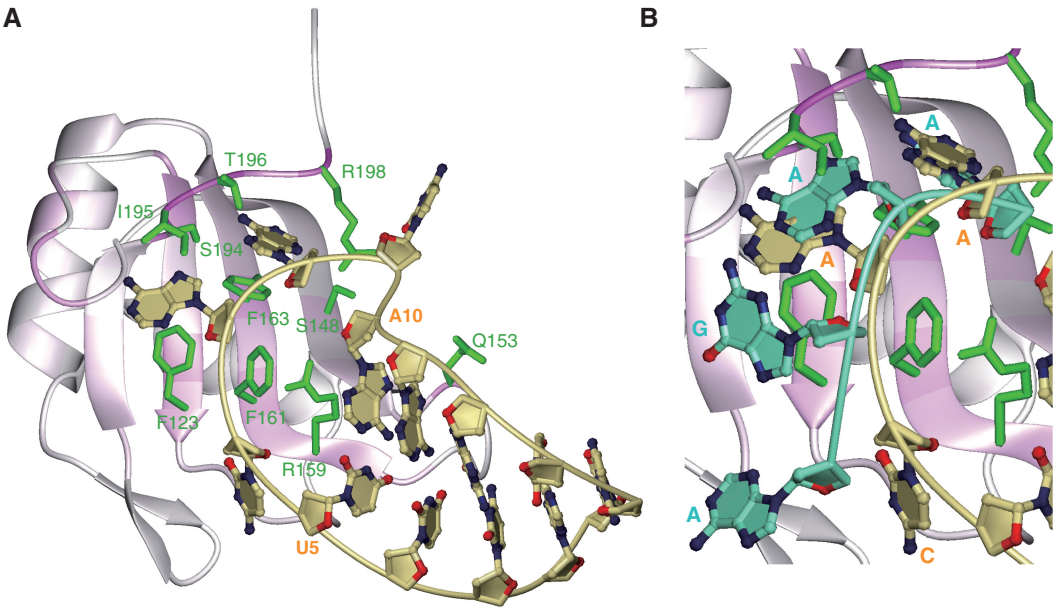

Figure 8. The two RNA binding modes of the hTra2-β RRM. (**A**) The model structure of the hTra2-β RRM in complex with the [5′-(GACUUCAACAAGUC)-3′] sequence. The protein structure is represented by a pink ribbon model, which is colored according to the magnitude of the chemical shift perturbation in Figure 4D. The side chains of the amino acid residues that undergo significant chemical shift changes upon binding to [5′-(GACUUCAACAAGUC)-3′] RNA are represented, and are colored green. The RNA is colored light yellow. In addition, the atoms of the RNA molecule are colored red (oxygen) and blue (nitrogen). (**B**) The [5′-(GAAGAA)-3′] sequence was superimposed on the modeled structure of the complex between the hTra2-β RRM and [5′-(GACUUCAACAAGUC)-3′], and a close-up view of the interaction surface of the hTra2-β RRM with each RNA molecule is represented. The [5′-(GAAGAA)-3′] RNA is colored light cyan.

residue on RNP2 (N1 position), and N2 was stacked with that on RNP1 (N2 position). In the case of the hTra2-β RRM, the bases of A5 and A6 occupy the space corresponding to the N1 and N2 positions of the canonical RRM, although the well-conserved aromatic amino-acid residue on RNP2 is missing. In addition, as in the canonical RRM, the backbone amide protons and carboxyl oxygen atoms of the N- and C-terminal extensions, as well as several side-chain atoms, are involved in the formation of specific hydrogen bonds to the two adenine bases (Figure 5D), as previously described (46).

Furthermore, the canonical RRM accommodates additional nucleotides that precede N1 and follow N2, referred to as N0 and N3, respectively. The N0 nucleotide is located on the β1 and β4 strands (N0′ position) or in a binding pocket formed by the β1–α1 and β2–β3 loop (N0″ position). The N3 nucleotide is located on the β2 strand (N3′ position) or is stacked on the N2 nucleotide (N3″ position). The molecular informatics analysis indicated that in the canonical RRMs, a uracil nucleotide frequently occupies the N0′ and N0″ positions (45), especially in the case of the N0′ position. In the hTra2-β RRM, the purine base of G4 occupies the position corresponding to the N0′ position in the canonical RRM. The unusually-positioned Phe123 enables the guanine base moiety to be situated in close proximity to the following adenine base moiety, for the formation of the hydrogen bond network between these base moieties, G4 and A5, along with Arg190 and Asp192. This interaction is quite important for the recognition by the hTra2-β RRM. Thus, the replacement of the guanine nucleotide with another type of nucleotide is expected to disrupt the attachment of the A5 nucleotide on the β-sheet surface and dramatically weaken the interaction between the hTra2-β RRM and RNA molecules. Actually, the hTra2-β RRM could not bind tightly to the [5′-(AAAAAA)-3′] sequence.

Consequently, in the hTra2-β RRM, the consecutive GAA nucleotides are located at the N0′, N1, and N2 positions, respectively, and the N0′ position plays a crucial role in the recognition of the purine stretch. We found RRMs that recognize consecutive purine stretches containing guanine nucleotides as target RNA sequences (UAGG sequence for the hnRNP A1 RRM1, and GAGA sequence for the Prp24 RRM2). In the hnRNP A1 RRM1, the AGG nucleotides are located at the N1, N2 and N3′ positions, respectively (42). Similarly, in the Prp24 RRM2, the GAG nucleotides occupy the N1, N2 and N3′ positions, respectively (47). Therefore, among the RRMs that recognize such a purine stretch, the hTra2-β RRM is considered to be unique, in that the N0′ position is utilized as the crucial recognition site for the purine nucleotide.

The two RNA binding modes of the hTra2-β RRM

The weak binding of the hTra2-β RRM to the [5′-(UCAAU)-3′] sequence can also be explained by the disruption of the hydrogen bond network at the N0′ position, although the CAA sequence is a target candidate for hTra2-β. In order to resolve this apparent contradiction, we investigated the binding of the hTra2-β RRM to the longer RNA sequence, [5′-(GACUUCAACAAGUC)-3′]. Interestingly, the hTra2-β RRM bound this RNA

Downloaded from nar.oxfordjournals.org at Stadt und Universitatsbibiothek / Section Medizinische Hauptbibliothek on March 1, 2011

sequence as tightly as the [5′-(GAAGAA)-3′] sequence, and the titration experiment using the 2D [^{1}H, ^{15}N]-HSQC spectra for the [5′-(GACUUCA ACAAGUC)-3′] sequence revealed that, unlike the [5′-(GAAGAA)-3′] sequence, several resonances originating from the β2–β3 loop were affected. These results indicate that the β2–β3 loop is involved in the recognition of the longer RNA sequence, and compensates for the decreased binding affinity for the [5′-(UCAAC)-3′] sequence. In addition, the chemical shift perturbations on the β4 strand and in the bottom region of the β1 strand, where A3 and G4 are located, are smaller in the case of the [5′-(GACUUCAAC AAGUC)-3′] sequence. This suggests that the binding mode on the β-sheet surface is different, and that the pocket for the A3 and G4 base moieties is not utilized. In addition, as described above, the [5′-(GACUUCAACA AGUC)-3′] sequence forms a stem-loop structure, and the CAAC sequence is in the single-stranded form. We found that the stem structure of the 14-mer RNA molecule is stabilized upon binding to the hTra2-β RRM.

When we searched for the complex structures of the RRMs that have the canonical aromatic alignment on the β-sheet surface and recognize an RNA fragment containing an AA dinucleotide, we found that this was the case for the RRMs of Poly-A binding protein (PABP) and RBMY (48,49). Considering the *syn-anti* conformations of these two nucleotides, the locations of these adenosine nucleotides on the β-sheet surface are very similar between the hTra2-β RRM and the RBMY RRM (Figure 7B and C). In the case of the RBMY RRM, the cytidine nucleotide just preceding the AA dinucleotide (cytidine nucleotide) is located near the edge of the β1 strand (N0″ position), and thus is rather far away from the base moiety of the following adenosine nucleotide. Therefore, the stem-loop structure is considered to be necessary to tightly fix the target RNA on the β-sheet surface of the RBMY RRM. The hTra2-β RRM may recognize the CAA sequence integrated within the stem-loop structure in a similar manner.

On the basis of a comparison with the RBMY RRM in the complex with the target RNA and the results of several NMR experiments, we suggested a model structure of the hTra2-β RRM in complex with [5′-(GACUUCAACAAG UC)-3′], as shown in Figure 8. In the model, the hTra2-β RRM recognizes the single-stranded region of the [5′-(GA CUUCAACAAGUC)-3′] RNA (mainly the AA dinucleotide) on its β-sheet surface, and interacts with the stem region of RNA by using the loop region between the β2 and β3 strands of the hTra2-β RRM. Therefore, the stem structure of the [5′-(GACUUCAACAAGUC)-3′] may interact with the β2–β3 loop, and assist in the interaction between the hTra2-β RRM and the 14-mer RNA molecule (Figure 8). The hTra2-β RRM may recognize two RNA sequences according to the structure of the RNA molecule: in an extended form, as in the AGAA sequence, or in a stem-loop structure, as observed in the [5′-(GACUUCAACAAGUC)-3′] sequence. Furthermore, it is conceivable that hTra2-β binds to the GAA sequence to anneal the secondary structure of the target RNA, while it stabilizes the stem-loop structure by interacting with the CAA sequence.

The present structural study revealed the dual RNA recognition and discrimination mechanisms of the hTra2-β protein. Since the hTra2-β protein functions together with other splicing factors, precise structural analyses of these factors, including the RNA molecules, will be required to clarify the mechanism of the alternative splicing system.

ACCESSION CODES

The atomic coordinates for the ensembles of 20 energy-refined NMR conformers, representing the solution structures of the hTra2-β RRM and the hTra2-β RRM in complex with [5′-(GAAGAA)-3′], have been deposited in the Protein Data Bank with the accession codes 2RRB and 2RRA, respectively.

SUPPLEMENTARY DATA

Supplementary Data are available at NAR Online.

ACKNOWLEDGEMENTS

The authors thank Dr T. Nagata and Ms S. Suzuki for help with the NMR data analysis, structure calculations and structure refinement. They also thank Dr T. Matsuda, Ms Y. Tomo, Dr M. Aoki, Dr T. Nagira, Dr E. Seki, Mr K. Hanada, Mr M. Ikari, Ms Y. Fujikura, Ms Y. Tomabechi and Ms Y. Kamewari-Hayami for sample preparation; and Ms A. Ishii and Ms T. Nakayama for help with the manuscript preparation.

FUNDING

RIKEN Structural Genomics/Proteomics Initiative (RSGI), and by the National Project on Protein Structural and Functional Analyses of the Ministry of Education, Culture, Sports, Science and Technology of Japan. This work was also supported by grants to Y.M. from the Human Frontier Science Program (HFSP) and the Ministry of Educations Culture, Sports, Science and Technology of Japan. P.G. was supported by a grant-in-aid for Scientific Research of the Japan Society for the Promotion of Science (JSPS) and by the Volkswagen Foundation. Funding for open access charge: RIKEN.

Conflict of interest statement. None declared.

REFERENCES

1. Bourgeois,C.F., Lejeune,F. and Stevenin,J. (2004) Broad specificity of SR (serine/arginine) proteins in the regulation of alternative splicing of pre-messenger RNA. *Prog. Nucleic Acid Res. Mol. Biol.*, **78**, 37–88.
2. Zheng,Z.M. (2004) Regulation of alternative RNA splicing by exon definition and exon sequences in viral and mammalian gene expression. *J. Biomed. Sci.*, **11**, 278–294.
3. Inoue,K., Hoshijima,K., Higuchi,I., Sakamoto,H. and Shimura,Y. (1992) Binding of the Drosophila transformer and transformer-2 proteins to the regulatory elements of doublesex primary

Downloaded from nar.oxfordjournals.org at Stadt und Universitatsbibliothek / Section Medizinische Hauptbibliothek on March 1, 2011

transcript for sex-specific RNA processing. *Proc. Natl Acad. Sci. USA*, **89**, 8092–8096.
4. Kondo,S., Yamamoto,N., Murakami,T., Okumura,M., Mayeda,A. and Imaizumi,K. (2004) Tra2β, SF2/ASF and SRp30c modulate the function of an exonic splicing enhancer in exon 10 of tau pre-mRNA. *Genes Cells*, **9**, 121–130.
5. Sumner,C.J. (2007) Molecular mechanisms of spinal muscular atrophy. *J. Child. Neurol.*, **22**, 979–989.
6. Soulard,M., Della Valle,V., Siomi,M.C., Pinol-Roma,S., Codogno,P., Bauvy,C., Bellini,M., Lacroix,J.C., Monod,G., Dreyfuss,G. *et al.* (1993) hnRNP G: sequence and characterization of a glycosylated RNA-binding protein. *Nucleic Acids Res.*, **21**, 4210–4217.
7. Screaton,G.R., Caceres,J.F., Mayeda,A., Bell,M.V., Plebanski,M., Jackson,D.G., Bell,J.I. and Krainer,A.R. (1995) Identification and characterization of three members of the human SR family of pre-mRNA splicing factors. *EMBO J.*, **14**, 4336–4349.
8. Krainer,A.R., Conway,G.C. and Kozak,D. (1990) The essential pre-mRNA splicing factor SF2 influences 5′ splice site selection by activating proximal sites. *Cell*, **62**, 35–42.
9. Ge,H., Zuo,P. and Manley,J.L. (1991) Primary structure of the human splicing factor ASF reveals similarities with Drosophila regulators. *Cell*, **66**, 373–382.
10. Tacke,R., Tohyama,M., Ogawa,S. and Manley,J.L. (1998) Human Tra2 proteins are sequence-specific activators of pre-mRNA splicing. *Cell*, **93**, 139–148.
11. Tran,Q., Coleman,T.P. and Roesser,J.R. (2003) Human transformer 2beta and SRp55 interact with a calcitonin-specific splice enhancer. *Biochim. Biophys. Acta*, **1625**, 141–152.
12. Nagai,K., Oubridge,C., Ito,N., Avis,J. and Evans,P. (1995) The RNP domain: a sequence-specific RNA-binding domain involved in processing and transport of RNA. *Trends Biochem. Sci.*, **20**, 235–240.
13. Perez-Canadillas,J.M. and Varani,G. (2001) Recent advances in RNA-protein recognition. *Curr. Opin. Struct. Biol.*, **11**, 53–58.
14. Clery,A., Blatter,M. and Allain,F.H. (2008) RNA recognition motifs: boring? Not quite. *Curr. Opin. Struct. Biol.*, **18**, 290–298.
15. Finn,R.D., Mistry,J., Schuster-Bockler,B., Griffiths-Jones,S., Hollich,V., Lassmann,T., Moxon,S., Marshall,M., Khanna,A., Durbin,R. *et al.* (2006) Pfam: clans, web tools and services. *Nucleic Acids Res.*, **34**, D247–D251.
16. Finn,R.D., Tate,J., Mistry,J., Coggill,P.C., Sammut,S.J., Hotz,H.R., Ceric,G., Forslund,K., Eddy,S.R., Sonnhammer,E.L. *et al.* (2008) The Pfam protein families database. *Nucleic Acids Res.*, **36**, D281–D288.
17. Kielkopf,C.L., Lucke,S. and Green,M.R. (2004) U2AF homology motifs: protein recognition in the RRM world. *Genes Dev.*, **18**, 1513–1526.
18. Kigawa,T., Yabuki,T., Matsuda,N., Matsuda,T., Nakajima,R., Tanaka,A. and Yokoyama,S. (2004) Preparation of Escherichia coli cell extract for highly productive cell-free protein expression. *J. Struct. Funct. Genomics*, **5**, 63–68.
19. Kigawa,T., Yabuki,T., Yoshida,Y., Tsutsui,M., Ito,Y., Shibata,T. and Yokoyama,S. (1999) Cell-free production and stable-isotope labeling of milligram quantities of proteins. *FEBS Lett.*, **442**, 15–19.
20. Matsuda,T., Koshiba,S., Tochio,N., Seki,E., Iwasaki,N., Yabuki,T., Inoue,M., Yokoyama,S. and Kigawa,T. (2007) Improving cell-free protein synthesis for stable-isotope labeling. *J. Biomol. NMR*, **37**, 225–229.
21. Bax,A. (1994) Multidimensional nuclear magnetic resonance methods for protein studies. *Curr. Opin. Struct. Biol.*, **4**, 738–744.
22. Kay,L.E. (1997) NMR methods for the study of protein structure and dynamics. *Biochem. Cell Biol.*, **75**, 1–15.
23. Delaglio,F., Grzesiek,S., Vuister,G.W., Zhu,G., Pfeifer,J. and Bax,A. (1995) NMRPipe: a multidimensional spectral processing system based on UNIX pipes. *J. Biomol. NMR*, **6**, 277–293.
24. Johnson,B.A. (2004) Using NMRView to visualize and analyze the NMR spectra of macromolecules. *Methods Mol. Biol.*, **278**, 313–352.
25. Kobayashi,N., Iwahara,J., Koshiba,S., Tomizawa,T., Tochio,N., Güntert,P., Kigawa,T. and Yokoyama,S. (2007) KUJIRA, a package of integrated modules for systematic and interactive analysis of NMR data directed to high-throughput NMR structure studies. *J. Biomol. NMR*, **39**, 31–52.
26. Pierre Plateau,M.G. (1982) Exchangeable proton NMR without base-line distortion, using new strong-pulse sequences. *J. Am. Chem. Soc.*, **104**, 7310–7311.
27. Farrow,N.A., Muhandiram,R., Singer,A.U., Pascal,S.M., Kay,C.M., Gish,G., Shoelson,S.E., Pawson,T., Forman-Kay,J.D. and Kay,L.E. (1994) Backbone dynamics of a free and phosphopeptide-complexed Src homology 2 domain studied by ^{15}N NMR relaxation. *Biochemistry*, **33**, 5984–6003.
28. Herrmann,T., Güntert,P. and Wüthrich,K. (2002) Protein NMR structure determination with automated NOE assignment using the new software CANDID and the torsion angle dynamics algorithm DYANA. *J. Mol. Biol.*, **319**, 209–227.
29. Güntert,P. (2009) Automated structure determination from NMR spectra. *Eur. Biophys. J.*, **38**, 129–143.
30. Güntert,P., Mumenthaler,C. and Wüthrich,K. (1997) Torsion angle dynamics for NMR structure calculation with the new program DYANA. *J. Mol. Biol.*, **273**, 283–298.
31. Powers,R., Garrett,D.S., March,C.J., Frieden,E.A., Gronenborn,A.M. and Clore,G.M. (1993) The high-resolution, three-dimensional solution structure of human interleukin-4 determined by multidimensional heteronuclear magnetic resonance spectroscopy. *Biochemistry*, **32**, 6744–6762.
32. Tsuda,K., Kuwasako,K., Takahashi,M., Someya,T., Inoue,M., Terada,T., Kobayashi,N., Shirouzu,M., Kigawa,T., Tanaka,A. *et al.* (2009) Structural basis for the sequence-specific RNA-recognition mechanism of human CUG-BP1 RRM3. *Nucleic Acids Res.*, **37**, 5151–5166.
33. Case,D.A., Cheatham,T.E. 3rd, Darden,T., Gohlke,H., Luo,R., Merz,K.M. Jr, Onufriev,A., Simmerling,C., Wang,B. and Woods,R.J. (2005) The Amber biomolecular simulation programs. *J. Comput. Chem.*, **26**, 1668–1688.
34. Laskowski,R.A., Rullmann,J.A., MacArthur,M.W., Kaptein,R. and Thornton,J.M. (1996) AQUA and PROCHECK-NMR: programs for checking the quality of protein structures solved by NMR. *J. Biomol. NMR*, **8**, 477–486.
35. Koradi,R., Billeter,M. and Wüthrich,K. (1996) MOLMOL: a program for display and analysis of macromolecular structures. *J. Mol. Graph.*, **14**, 51–55, 29–32.
36. Rao,J.N., Schweimer,K., Wenzel,S., Wohrl,B.M. and Rosch,P. (2008) NELF-E RRM undergoes major structural changes in flexible protein regions on target RNA binding. *Biochemistry*, **47**, 3756–3761.
37. Morozova,N., Allers,J., Myers,J. and Shamoo,Y. (2006) Protein-RNA interactions: exploring binding patterns with a three-dimensional superposition analysis of high resolution structures. *Bioinformatics*, **22**, 2746–2752.
38. Mathews,D.H., Sabina,J., Zuker,M. and Turner,D.H. (1999) Expanded sequence dependence of thermodynamic parameters improves prediction of RNA secondary structure. *J. Mol. Biol.*, **288**, 911–940.
39. Zuker,M. (2003) Mfold web server for nucleic acid folding and hybridization prediction. *Nucleic Acids Res.*, **31**, 3406–3415.
40. Auweter,S.D., Fasan,R., Reymond,L., Underwood,J.G., Black,D.L., Pitsch,S. and Allain,F.H. (2006) Molecular basis of RNA recognition by the human alternative splicing factor Fox-1. *EMBO J.*, **25**, 163–173.
41. Oubridge,C., Ito,N., Evans,P.R., Teo,C.H. and Nagai,K. (1994) Crystal structure at 1.92 A resolution of the RNA-binding domain of the U1A spliceosomal protein complexed with an RNA hairpin. *Nature*, **372**, 432–438.
42. Ding,J., Hayashi,M.K., Zhang,Y., Manche,L., Krainer,A.R. and Xu,R.M. (1999) Crystal structure of the two-RRM domain of hnRNP A1 (UP1) complexed with single-stranded telomeric DNA. *Genes Dev.*, **13**, 1102–1115.
43. Oberstrass,F.C., Auweter,S.D., Erat,M., Hargous,Y., Henning,A., Wenter,P., Reymond,L., Amir-Ahmady,B., Pitsch,S., Black,D.L. *et al.* (2005) Structure of PTB bound to RNA: specific binding and implications for splicing regulation. *Science*, **309**, 2054–2057.
44. Handa,N., Kukimoto-Niino,M., Akasaka,R., Kishishita,S., Murayama,K., Terada,T., Inoue,M., Kigawa,T., Kose,S., Imamoto,N. *et al.* (2006) The crystal structure of mouse Nup35

Downloaded from nar.oxfordjournals.org at Stadt und Universitätsbibliothek / Section Medizinische Hauptbibliothek on March 1, 2011

reveals atypical RNP motifs and novel homodimerization of the RRM domain. *J. Mol. Biol.*, **363**, 114–124.
45. Auweter,S.D., Oberstrass,F.C. and Allain,F.H. (2006) Sequence-specific binding of single-stranded RNA: is there a code for recognition? *Nucleic Acids Res.*, **34**, 4943–4959.
46. Myers,J.C. and Shamoo,Y. (2004) Human UP1 as a model for understanding purine recognition in the family of proteins containing the RNA recognition motif (RRM). *J. Mol. Biol.*, **342**, 743–756.
47. Martin-Tumasz,S., Reiter,N.J., Brow,D.A. and Butcher,S.E. (2010) Structure and functional implications of a complex containing a segment of U6 RNA bound by a domain of Prp24. *RNA*, **16**, 792–804.
48. Deo,R.C., Bonanno,J.B., Sonenberg,N. and Burley,S.K. (1999) Recognition of polyadenylate RNA by the poly(A)-binding protein. *Cell*, **98**, 835–845.
49. Skrisovska,L., Bourgeois,C.F., Stefl,R., Grellscheid,S.N., Kister,L., Wenter,P., Elliott,D.J., Stevenin,J. and Allain,F.H. (2007) The testis-specific human protein RBMY recognizes RNA through a novel mode of interaction. *EMBO Rep.*, **8**, 372–379.

Downloaded from nar.oxfordjournals.org at Stadt und Universitatsbibliothek / Section Medizinische Hauptbibliothek on March 1, 2011